Regulating d^0 Transition Metal and Facilitating the High-Performance Li-excess Cation-Disorder Rocksalt Cathode Materials

Hui Song,[a] Wenyong Xie,[a] Yinfeng Tian,[a] Min Guo,[a] Tao Wang,[a] Dianwu Kang,[a] Min Jia,[a] Xiaoyu Zhang,*[a]*

[a] School of Material Science and Engineering, Jiangsu University, Zhenjiang, 212013, China

Corresponding Author

Min Jia: mjia@ujs.edu.cn

Xiaoyu Zhang: x.zhang@ujs.edu.cn

Key Words

Cation-disordered rocksalts; Li-excess cathodes; d^0 transition metal effect; design principle; Li^+ diffusion kinetics

Experimental Section

Synthesis:

$Li_{1.2}Mn_{0.4}^{3+}Ti_xMn_{0.4-x}^{4+}O_2$ (x=0,0.05,0.1,0.2,0.3,0.35) was synthesized by a conventional solid phase sintering method using the precursors TiO_2 (Sigma-Aldrich 99%), Mn_2O_3 (Sigma-Aldrich 99.9%) and MnO_2 (Sigma-Aldrich 99.9%) and a 10% excess of Li_2CO_3 (Sigma-Aldrich 99%). After grinding in a mortar for 30 minutes, the stoichiometric ratio correct precursor was added to an agate ball mill jar. The precursors were ball milled with anhydrous ethanol at 400 rpm for 12 h using a planetary ball mill (RETSCH-PM100). The well-mixed precursors were dried in an oven for 12 h and pressed into flakes. The samples were heated at a ramp rate of 5°C min^{-1} and calcined in an Ar atmosphere quartz tube furnace at 950°C for 16 hours. The sintered samples were ground to powder and placed in a glove box and set aside.

Material Characterization.

X-ray diffraction (XRD) patterns were obtained using a Bruker D8 Advance (Cu Kα radiation, λ = 1.5406 Å) with experimental parameters in the 2θ range of 10-85°.

Cathode crystal detail parameters were obtained using the Rietveld refinement method under GSAS-II software. The schematic representation of the crystal structure was obtained using VESTA software. The stoichiometric composition of the Cathodes material was quantified using Thermo ICAP PRO inductively coupled plasma mass spectrometry (ICP-MS). High-resolution transmission electron microscopy (HRTEM) was used to observe the microstructural features of the materials, including energy-dispersive X-ray spectroscopy (EDS) for chemical composition. Valence changes of elements in the cathode material were analyzed by X-ray photoelectron spectroscopy (XPS) using a Thermo Fisher Nexsa instrument.

Electrochemical Measurements.

First, the active material and acetylene black were mixed in a mass ratio of 8:2 using a planetary ball mill (FRITSCH-6) under inert gas protection in a zirconia ball milling tank at 600 rpm for 3 hours. Then, the mixed active material (80 wt%), polyvinylidene fluoride (10 wt%), and acetylene black (10 wt%) were uniformly coated on an aluminum foil using N-methyl pyrrolidone (NMP) as a solvent, and the coated positive electrode was kept in a vacuum oven at 80 °C for 12 hours. The electrolyte was a solution of 1 M $LiPF_6$ dissolved in EC and DMC (1:1 mass ratio).. The septum was a porous polypropylene membrane (Celgard-2400), and the negative electrode was a lithium sheet. The CR2032-type coin cell was assembled in an argon-filled glovebox and the electrochemical properties were tested on a battery test system (LandBT2001A) at room temperature over a voltage window of 1.5-4.8 V. The galvanostatic intermittent titration technique (GITT) measurements were performed on the same equipment at a current density of 20 mA g^{-1} for 30 minutes and then rested for 4 hours to reach steady state. The corresponding diffusion coefficients were calculated from these curves. The diffusion coefficients were calculated based on Fick's second law. To calculate the diffusion coefficients of Li^+ in different charging-discharging states, use the following equation[1]：

$$D_{Li^+} = \frac{4}{\pi\tau}\left(\frac{m_B V_M}{M_B A}\right)^2\left(\frac{\Delta E_S}{\tau\left(dE_\tau/d\sqrt{\tau}\right)}\right)^2, \left(\tau \ll L^2/D_{Li^+}\right)$$

When the applied constant current is linearly related to the relaxation time, the

above equation can be further simplified to the following equation:

$$D_{Li^+} = \frac{4}{\pi\tau}\left(\frac{m_B V_M}{M_B A}\right)^2\left(\frac{\Delta E_S}{\Delta E_\tau}\right)^2$$

DFT Computations.

We perform period-density generalized function theory calculations using the VASP code and the projector augmented wave (PAW) method to represent electron-ion interactions, using the Perdew-Burke-Ernzerhof (PBE) generalized function as the electron exchange correlation function.[2]

The initial disordered structure is created by the SQS module utilizing the Monte Carlo algorithm in the ATAT package[3, 4]. Special quasirandom structures (SQSs) are developed to describe the entire disordered phase using multiple characteristic local structures, or clusters. This is achieved by randomly sampling the clusters' correlation function, which generates a cell that can be computed by the Vienna Ab initio Simulation Package (VASP)[5]. The concept of the clusters' correlation function is derived from the cluster expansion formalism, which denotes the multiplicity of site occupation by each class of clusters, denoted by α. The specific formulas are as follows:

$$\prod_\alpha = \frac{1}{M_i}\sum_{\sigma_i}^{clusters}\prod_i^{sites}\gamma_{\alpha_i,M_i}(\sigma_i)$$

The symbol $\sigma_i(0\sim M_{i=1})$ indicates that there are M_i different chemical species occupying site i. The symbol α represents a cluster consisting of a list of sites, while $0\sim M_{i-1}\cdot\gamma_{\alpha_{i,M_i}}(\sigma_i)$ represents the occupation of sites, which is related to the Ising model $(\gamma_{\alpha_{i,M_i}}(\sigma_i)\varepsilon\{-1,+1\} in\ binary\ systems)$[6] This study used the SQS method to determine the disordered configurations of two materials, $Li_{1.2}Mn_{0.7}Ti_{0.1}O_2(MT_{0.1})$ and $Li_{1.2}Mn_{0.5}Ti_{0.3}O_2(MT_{0.3})$. These materials have a rocksalt structure and contain lithium, manganese, and titanium ions in their crystal lattice. The SQS method imposes constraints on the random structure obtained by the objective function, based on the pair range up to 7 Å, triple range up to 4.1 Å, and quadruple range up to 4.1 Å. Using the conventional structure, we sampled the disordered configurations of these materials in a 5x3x1 supercell. In order to evaluate the degree of disorder of the constructed SQS

structure, we use an objective function as a criterion to calculate the difference between the correlation function of the SQS structure and the perfect disordered structure, taking into account the multiplicity and diameter of the clusters. The closer the objective function is to 0, the closer the SQS structure is to a perfectly disordered structure.[7]. The computationally generated structural models of the two DRXs materials are displayed in the supporting information, as shown in Figure. S12.

The constructed crystal unit consists of a 5×3×1 face-centered cubic lattice with a total atomic number of 120. The SQS of both assemblies were fully optimized by scanning the Brillouin zone with a 3×3×1 Monkhorst-Pack *k*-point lattice and a total force of less than 0.02 eV $Å^{-1}$. The Li^{+} diffusion barriers were calculated using the Climb-image-nudged elastic band (CI-NEB) method.

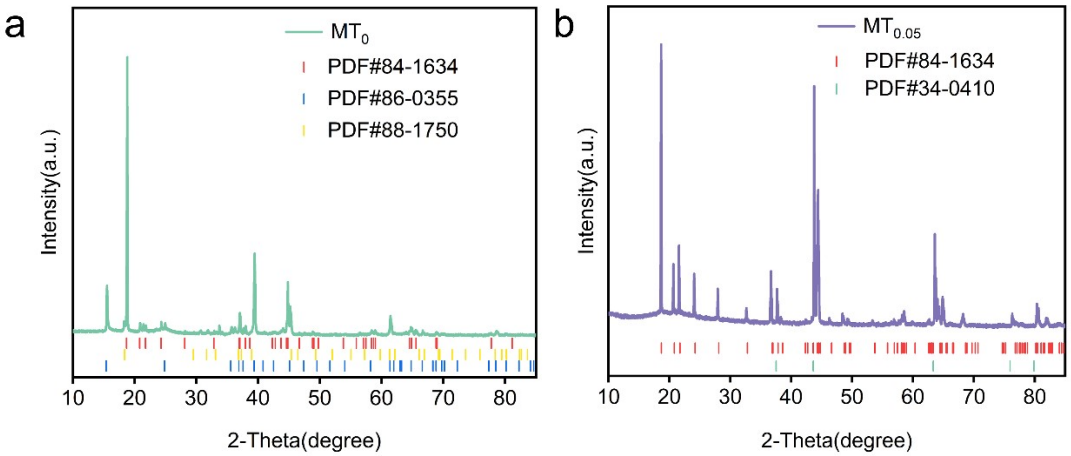

Fig.S1. XRD diffraction patterns of (a)MT_0 and (b) $MT_{0.05}$.

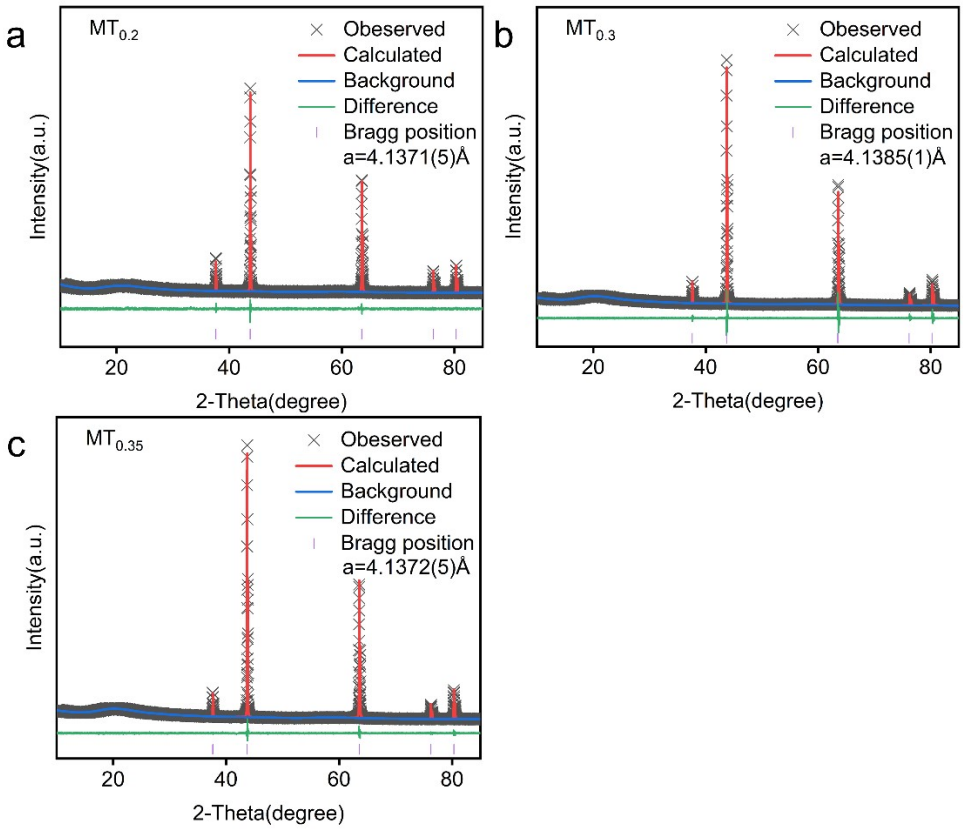

Fig.S2. Rietveld refinements of the XRD patterns of $MT_{0.2}$, $MT_{0.3}$ and $MT_{0.35}$.

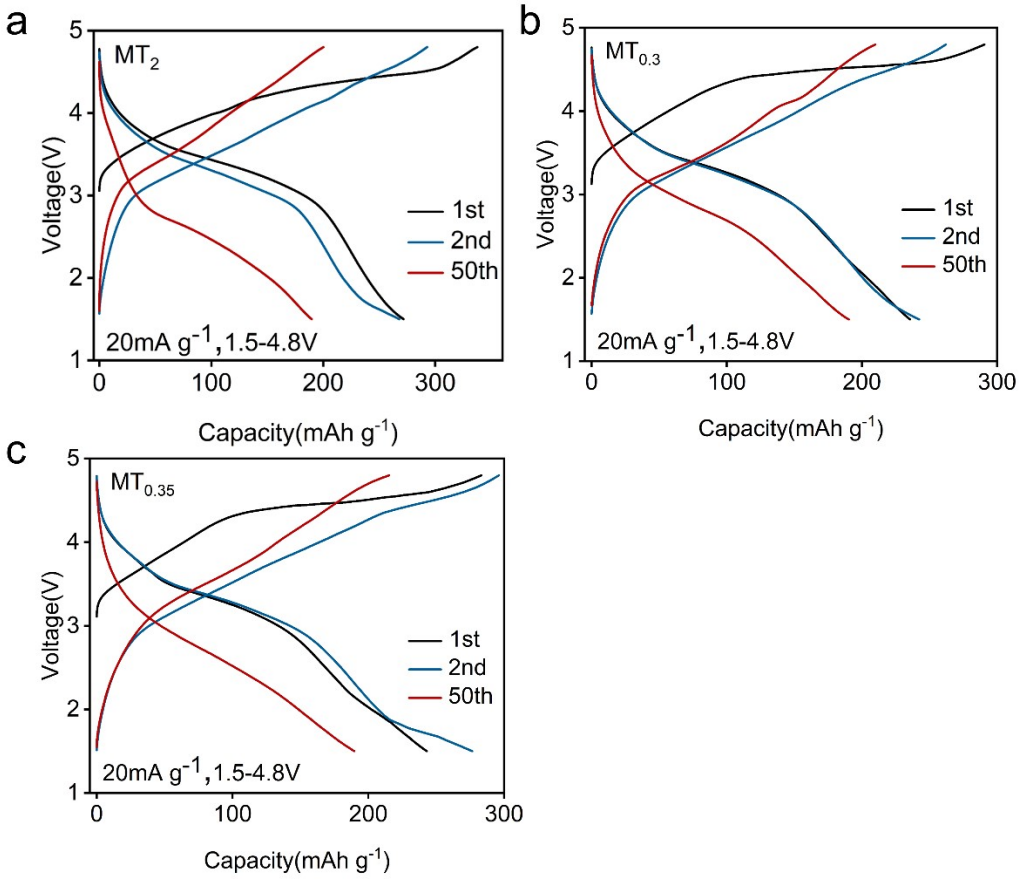

Fig.S3. Typical galvanostatic charge-discharge cycle curve of $MT_{0.2}$, $MT_{0.3}$ and $MT_{0.35}$.

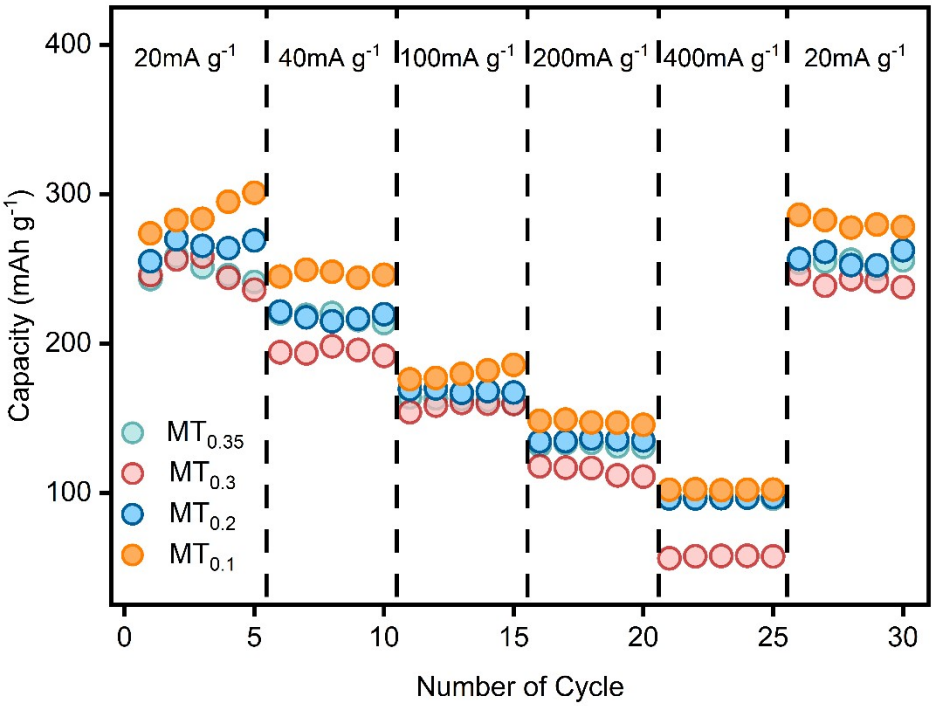

Fig.S4. Rate performance test of $MT_{0.1}$

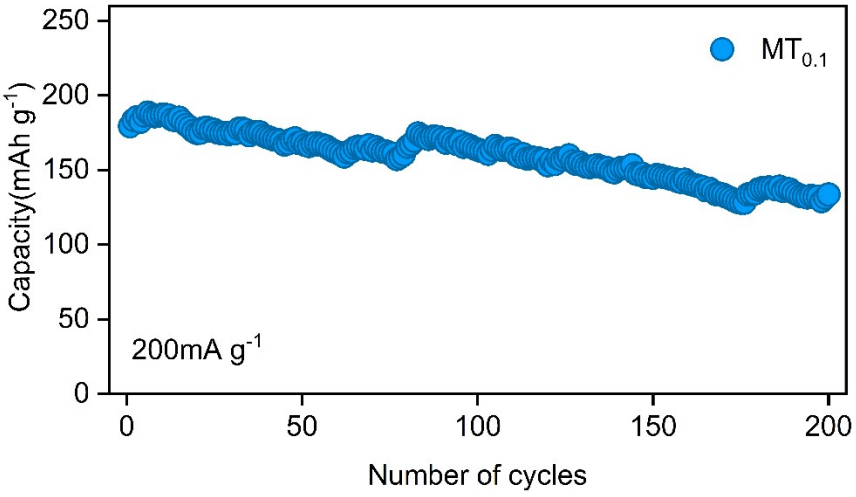

Fig.S5. Cycling performance test of $MT_{0.1}$ at 200 mA g^{-1} current density.

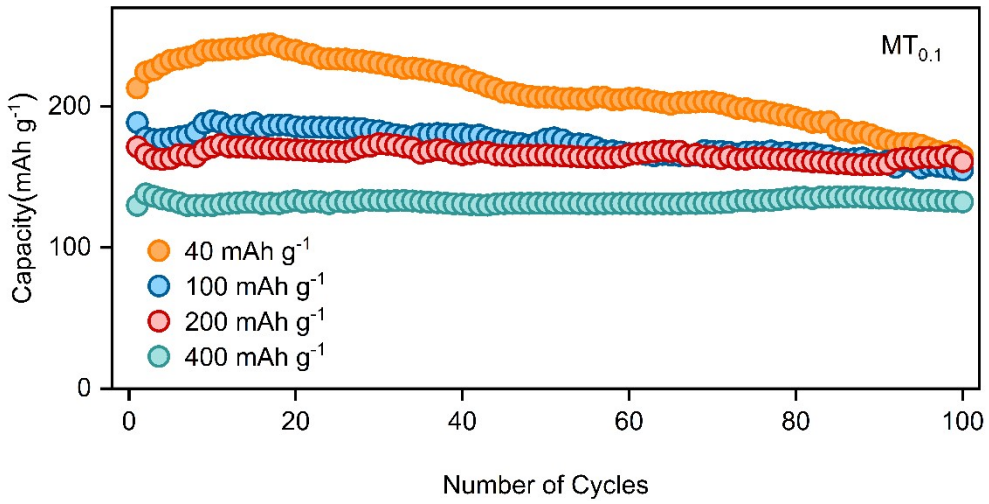

Fig.S6. Cycling performance of $MT_{0.1}$ sample at 40 mA g^{-1},100 mA g^{-1}, 200 mA g^{-1},400 mA g^{-1} current densities with voltage window of 1.5-4.8 V.

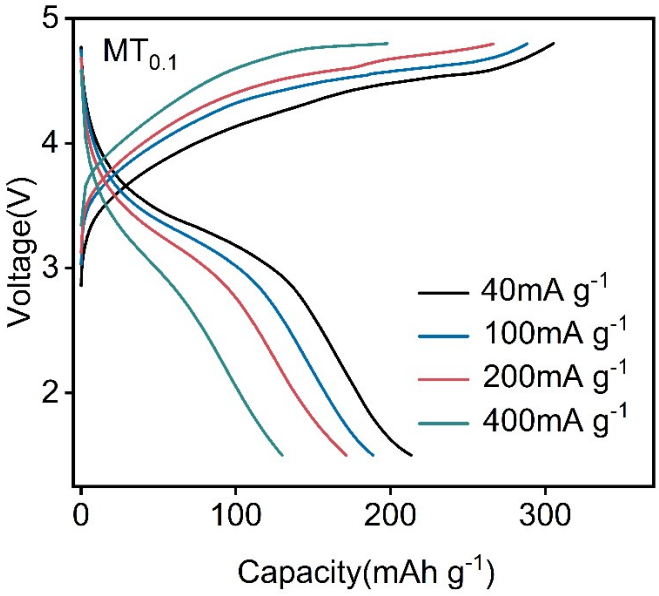

Fig.S7. Initial charge-discharge curves of $MT_{0.1}$ at different current densities.

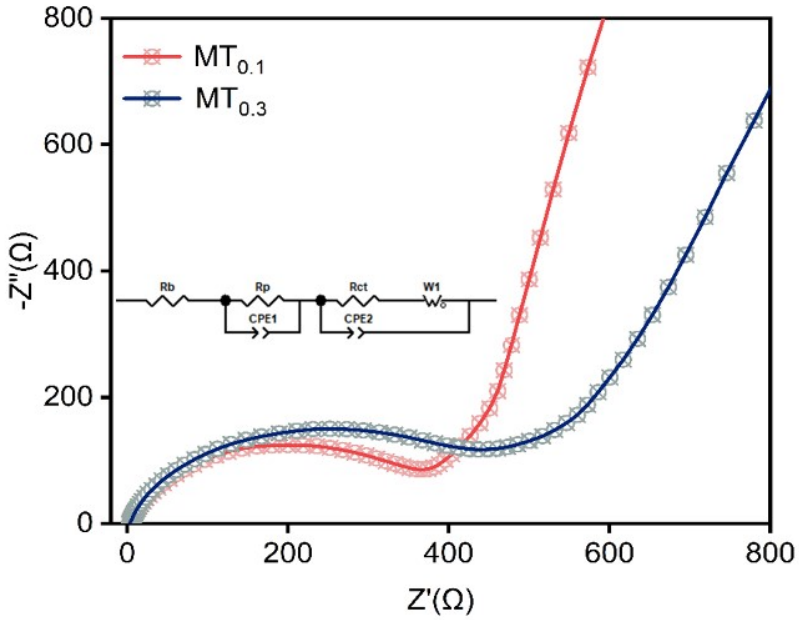

Fig. S8. The EIS spectrum of $MT_{0.1}$ and $MT_{0.3}$ after 5 cycles.

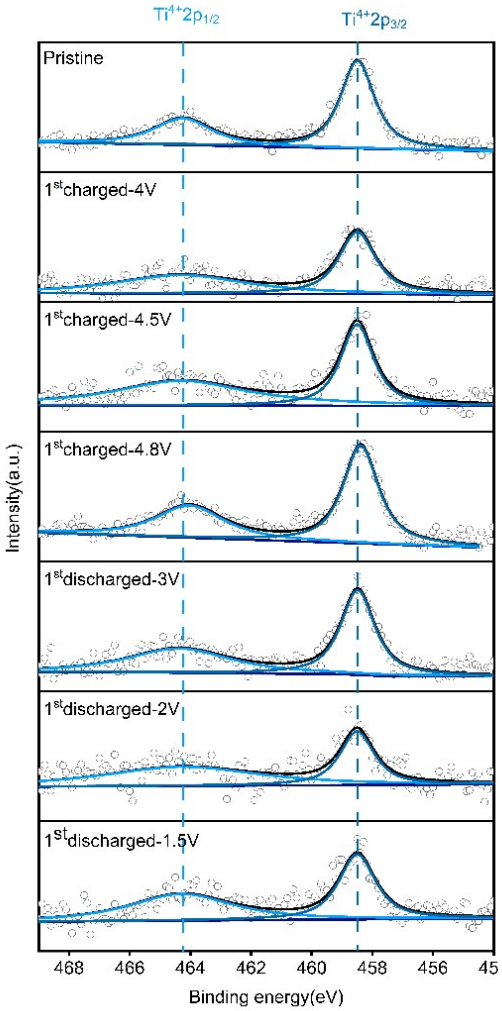

Fig.S9. XPS analysis of Ti 2p orbitals. The peak fitting of $MT_{0.1}$ includes both pristine materials and the first cycle.

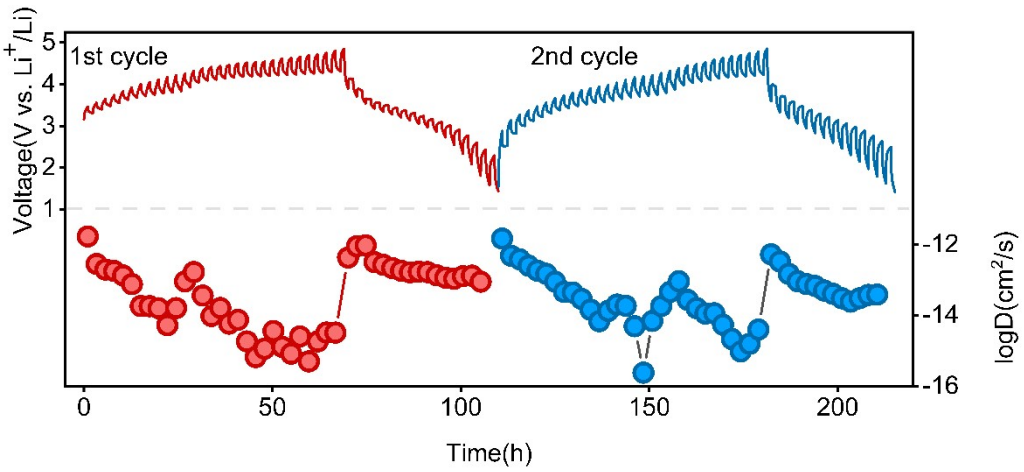

Fig.S10. GITT profiles and variation of the lithium ion diffusion coefficient (D_{Li+}) of $MT_{0.3}$ sample during the first cycle and second cycle processes.

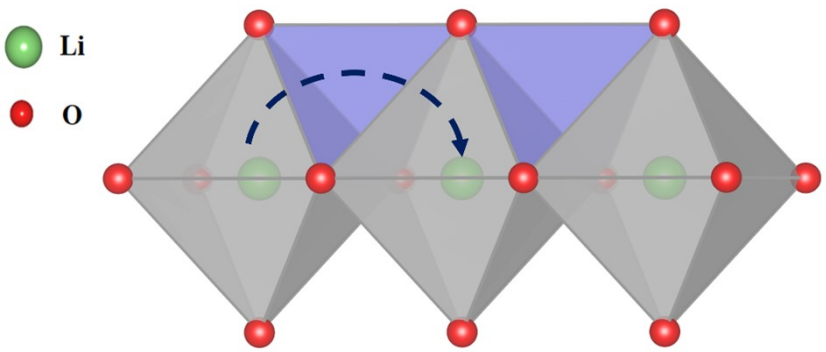

Fig.S11. Schematic diagram of Li^+ diffusion path.

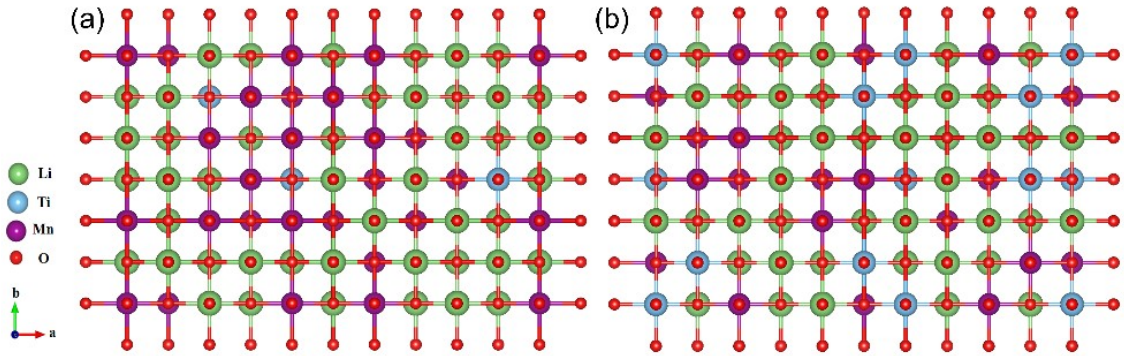

Fig. S12. Structural modeling of (a) $MT_{0.1}$, (b) $MT_{0.3}$.

Table S1. ICP measurement results of $MT_{0.1}$ samples for each element

Theoretical Formulation	Measurement of actual element ratios		
	Li	Mn	Ti
$Li_{1.2}Mn_{0.4}^{3+}Ti_{0.1}Mn_{0.3}^{4+}O_2$	1.187	0.684	0.098

Table S2. Lattice parameters of $MT_{0.1}$, $MT_{0.2}$, $MT_{0.3}$, $MT_{0.35}$

Material		$MT_{0.1}$	$MT_{0.2}$	$MT_{0.3}$	$MT_{0.35}$
Cation-disordered rocksalt structure ($Fm\bar{3}m$) (Å)	a	4.1469(1)	4.1371 (5)	4.1385(1)	4.1372(5)
R_{wp}(%)		4.87	7.34	6.18	4.76

Table S3. Comparison of electrochemical properties of reported manganese-based cationic-disordered rock salt materials.

Chemical formula	Initial capacity (mAh g^{-1})	Current density (mA g^{-1})	Number of cycles	Capacity retention(%)
This work:$MT_{0.1}$	283	20(1.5-4.8V)	50	86
$Li_{1.2}Mn_{0.4}Ti_{0.4}O_2$[8]	200	10(1.5-4.8V)	50	70
$Li_{1.1}Mn_{0.7}Ti_{0.2}O_2$[9]	240	30(1.5-4.8V)	15	≈92.5
$Li_{1.3}Nb_{0.3}Mn_{0.4}O_2$[10]	≈275	10(1.5-4.8V)	50	27
$Li_{1.15}Mn_{0.55}Ti_{0.3}O_2$[11]	≈210	20(2-4.8V)	100	83
$Li_{1.25}Nb_{0.15}Ti_{0.2}Mn_{0.4}O_2$[12]	276.1	10(1.5-4.8V)	50	≈36
$Li_{1.25}Mn(II)_{0.1667}Mn(III)_{0.5833}O_{1.3333}F_{0.6667}$[13]	256	20(1.5-5)	30	≈85

Reference:

1. H. Wang, X. Zhang, H. Zhang, Y. Tian, Q. Zhang, X. Zhang, S. Yang, M. Jia, H. Pan, C. Sheng and X. Yan, *ACS Applied Materials & Interfaces*, 2023, **15**, 11691-11702.
2. H. Wu, J. Dong, Y. Zhang, L. Lin, G. Gao, T. Li, X. Yi, B. Sa, J. Wang, L. Wang, J. Li, K. Amine, D. L. Peng and Q. Xie, *Advanced Functional Materials*, 2023, **33**, 2303707.
3. A. van de Walle, *Calphad*, 2009, **33**, 266-278.
4. A. van de Walle, *JOM*, 2013, **65**, 1523-1532.
5. G. Kresse and J. Furthmüller, *Physical Review B*, 1996, **54**, 11169-11186.
6. J. M. Sanchez, F. Ducastelle and D. Gratias, *Physica A: Statistical Mechanics and its Applications*, 1984, **128**, 334-350.
7. A. van de Walle, P. Tiwary, M. de Jong, D. L. Olmsted, M. Asta, A. Dick, D. Shin, Y. Wang, L. Q. Chen and Z. K. Liu, *Calphad*, 2013, **42**, 13-18.
8. D. Chen, J. Ahn, E. Self, J. Nanda and G. Chen, *Journal of Materials Chemistry A*, 2021, **9**, 7826-7837.
9. M. Diaz-Lopez, P. A. Chater, O. Proux, Y. Joly, J.-L. Hazemann, P. Bordet and V. Pralong, *Journal of Materials Chemistry A*, 2022, **10**, 17415-17423.
10. D. Chen, W. H. Kan and G. Chen, *Advanced Energy Materials*, 2019, **9**, 1901255.
11. Z. Cai, B. Ouyang, H.-M. Hau, T. Chen, R. Giovine, K. P. Koirala, L. Li, H. Ji, Y. Ha, Y. Sun, J. Huang, Y. Chen, V. Wu, W. Yang, C. Wang, R. J. Clément, Z. Lun and G. Ceder, *Nature Energy*, 2024, **9**, 27-36.
12. D. Chen, J. Wu, J. K. Papp, B. D. McCloskey, W. Yang and G. Chen, *Small*, 2020, **16**, 2000656.
13. Z. Lun, B. Ouyang, Z. Cai, R. J. Clément, D.-H. Kwon, J. Huang, J. K. Papp, M. Balasubramanian, Y. Tian, B. D. McCloskey, H. Ji, H. Kim, D. A. Kitchaev and G. Ceder, *Chem*, 2020, **6**, 153-168.